Carbon Nanotubes

Atomic-Step-Templated Formation of Single Wall Carbon Nanotube Patterns**

*Ariel Ismach, Lior Segev, Ellen Wachtel, and Ernesto Joselevich**

Following recent advances in the control of the electronic properties of nanowires,[1–4] nonlithographic organization of nanowire arrays on surfaces remains a critical prerequisite for the large-scale fabrication of nanoscale circuitry.[5,6] Current strategies[7] include the application of physical means, such as electric fields,[4,8,9] gas[10] and liquid[11,12] flows, and superlattices,[13] as well as chemical means including self-assembly[14,15] and biotemplated assembly.[16] Step decoration[15,17] is another attractive chemical approach that exploits the selective deposition of atoms, ions, or molecules at the oriented, periodic steps present on high-index crystalline surfaces. However, the general scheme, in which nanowire growth propagates transversely from the steps, is not compatible with nanowire materials that form by axial growth mechanisms, such as carbon nanotubes.[18–20] Here we demonstrate and characterize the longitudinally propagating decoration of atomic steps by a nanowire material. Single-wall carbon nanotubes that are catalytically produced on miscut C-plane sapphire wafers, grow along the 2-Å-high atomic steps of the vicinal α-Al_2O_3 (0001) surfaces to yield highly aligned, dense arrays of discrete, nanometer-wide, conducting or semiconducting wires on a dielectric material. The nanotubes reproduce the atomic features of the surface, such as steps, facets, and kinks. These findings open up the possibility of assembling nanotube architectures by atomic-scale surface engineering.

The phenomenon of atomic step decoration by single-wall carbon nanotubes (SWNTs) was first observed while investigating the effects of electric field and gas flow on the catalytic growth of SWNTs on different materials. Surprisingly, nanotubes grown on C-plane sapphire wafers, that is, α-Al_2O_3(0001) surfaces, showed the highest degree of alignment (Figures 1a, 2a, 3a–c, and 4a), but not in the directions of the field or the flow. When the same surface was precoated with a thin layer (20 nm) of amorphous SiO_2, the nanotubes were aligned with the electric field (Figure 1b), as previously observed on SiO_2-coated silicon.[8] This result indicated that the nanotubes grow in contact with the Al_2O_3 surface, which dictates their alignment. On the other hand, the nanotubes were not aligned along a particular crystallographic direction. Moreover, α-Al_2O_3 is a trigonal crystal of the $R\bar{3}c$ space group and an ideal α-Al_2O_3(0001) surface has C_3 symmetry, from which one would expect alignment in at least three directions, not one. These facts ruled out the possibility of lattice-oriented SWNT growth.[21] However, commercial "C-plane" sapphire wafers are often cut and polished in a plane that slightly deviates from the actual C plane. The resulting vicinal α-Al_2O_3(0001) surfaces are terminated with parallel, regularly spaced atomic steps.[22] The atomic steps of most materials are generally more reactive than atomically flat areas.[23] We then hypothesized that SWNTs could have grown along such atomic steps. This is proven below for the case where no electric field was applied. Application of an electric field was shown to have no effect.

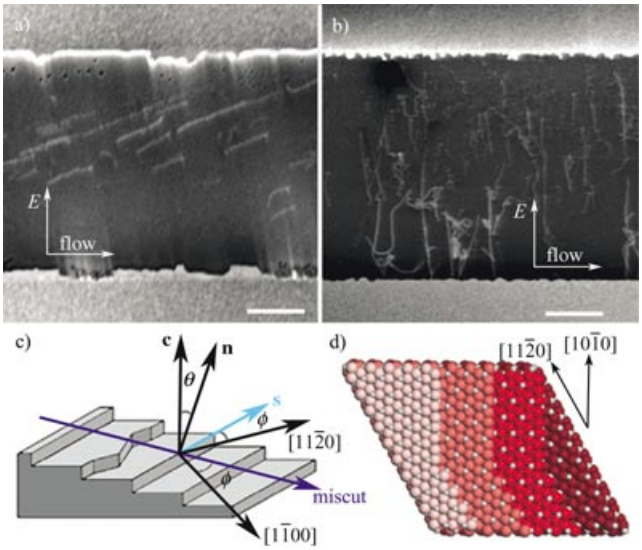

Figure 1. Alignment of SWNTs grown under an electric field (2×10^6 V m^{-1}) on sapphire (a) and on SiO_2-coated sapphire (b). The low-voltage field-emission SEM micrographs (scale bar: 5 μm) show the SWNTs (light) lying on the dielectric surfaces (dark), and the Pt electrodes (light, top and bottom). Arrows indicate the directions of the field *E* and flow. The alignment of the SWNTs on sapphire is unrelated to the electric field, whereas on the same sapphire that was precoated with 20 nm of amorphous SiO_2, the alignment is parallel to the electric field. c) Schematic representation of the atomic steps on vicinal α-Al_2O_3(0001), and definition of the step vector $\mathbf{s}=(\mathbf{c}/c)\times\mathbf{n}$, miscut inclination θ, and miscut azimuth ϕ. d) Idealized structure of atomic steps in different low-index directions, based on the bulk crystal structure, that is, without relaxation and reconstruction. Oxygen atoms (red) are colored darker at lower atomic layers.

The morphology and dynamics of vicinal α-Al_2O_3(0001) surfaces have been investigated by several research groups.[22,24] The atomic steps, with a height equal to one

[*] A. Ismach, L. Segev, Dr. E. Joselevich
Department of Materials and Interfaces
Weizmann Institute of Science, Rehovot 76100 (Israel)
Fax: (+972) 8-934-4138
E-mail: ernesto.joselevich@weizmann.ac.il
Dr. E. Wachtel
Chemical Research Infrastructure
Weizmann Institute of Science, Rehovot 76100 (Israel)

[**] We acknowledge A. Jorio, G. Dresselhaus, and M. S. Dresselhaus for Raman measurements. We thank L. Leiserowitz and M. Lahav for helpful discussions. This research was funded by the Israel Science Foundation, the U.S.–Israel Binational Science Foundation, and the Djanogly Center for New Scientists. E.J. holds the Dr. Victor Erlich Career Development Chair.

Supporting information (experimental methods, XRD data, statistical histograms, and a table of comprehensive results) for this article is available on the WWW under http://www.angewandte.org or from the author.

 © 2004 Wiley-VCH Verlag GmbH & Co. KGaA, Weinheim DOI: 10.1002/ange.200460356

sixth of the hexagonal unit cell, that is, $h = c/6 = 0.219$ nm, follow a general direction perpendicular to the miscut direction (Figure 1c). Their average spacing is $d = h/\sin\theta$ where θ is the miscut inclination. For convenience, we define a step vector $\mathbf{s} = (\mathbf{c}/c) \times \mathbf{n}$, where $\mathbf{c}$ is the principal lattice vector and $\mathbf{n}$ is a unit vector normal to the surface. Then, $\mathbf{s}$ points along the general step direction so that steps descend to the right, and its modulus equals the slope of the steps ($s = h/d$). We define the miscut azimuth ϕ ($-60° < \phi < +60°$) as the angle of $\mathbf{s}$ relative to the $[11\bar{2}0]$ direction, which is perpendicular to the $(11\bar{2}0)$ c-glide plane, so that the sign of ϕ expresses the handedness of chiral miscuts. The atomic step structure depends on the miscut azimuth ϕ. This is illustrated by Figure 1d, which represents different unreconstructed steps based on the bulk structure. The actual structure of the atomic steps is still unknown,[22] although the high-temperature reconstruction of α-$Al_2O_3(0001)$ surfaces was recently characterized.[25]

The characterization of a typical sample of aligned SWNTs on sapphire is shown in Figure 2. Figure 2a displays an AFM topographic image of the highly aligned SWNTs. The apparent diameter distribution of the SWNTs is 1.0 ± 0.4 nm, which is 0.2 nm smaller than the value determined from Raman spectra (1.2 ± 0.5 nm). An asymmetric double-exposure back-reflection X-ray diffraction (XRD) method was used to determine the orientations of both the lattice and the miscut of the α-$Al_2O_3(0001)$ substrate (Figure 2b), in which a long and a short exposure were taken before and after 180° rotation of the sample, respectively. The miscut inclination and azimuth are $\theta = 2.1 \pm 0.2°$ and $\phi = 0 \pm 5°$, respectively, and the general step direction, expressed by $\mathbf{s}$, matches the direction of the nanotube alignment. In addition, a destructive characterization by thermal annealing at 1100 °C in air (Figure 2c) was performed. Then, the thermodynamically unstable $c/6$ atomic steps, which could not be resolved by AFM, bunch into visible macrosteps with heights of c–$3c$.[22,24] The step orientation and miscut inclination are independently determined from these images, thus yielding results ($\theta = 1.9 \pm 0.2°$) similar to those obtained from XRD studies. The angular distribution of the nanotubes and macrosteps with respect to reference marks are $108 \pm 4°$ and $109 \pm 2°$, respectively (see Supporting Information for histograms). This precise coincidence is a clear indication of step decoration. The apparent reduction in SWNT height is consistent with the size of $c/6$ atomic steps.

Similar experiments were performed on about twenty samples of SWNTs grown on either side of seven different C-plane sapphire wafers of random miscut inclinations (up to $\theta = 4°$). Some representative results are displayed in Figure 3 (see Supporting Information for comprehensive data). In all cases, except for $\theta < 0.5°$, SWNTs grow parallel to the atomic steps and not to a particular lattice direction. The degree of alignment correlates with the miscut inclination. However, SWNTs grown on substrates having similar miscut inclinations show better alignment when the atomic steps run along low-index directions, such as $[11\bar{2}0]$ (Figure 3c) or $[10\bar{1}0]$ (Figure 3b), than along high-index directions (Figure 3d). This phenomenon may be attributed to the fact that straighter steps can have a closer interaction with the SWNTs. The density of the SWNT arrays also correlates with the value of θ. The samples with the lowest miscut inclination (Figure 3f) have visible atomic steps decorated by nanoparticles, but no nanotubes. The steps could play a role in stabilizing the catalyst nanoparticles, so that a higher density of steps leads to a higher yield of SWNTs.

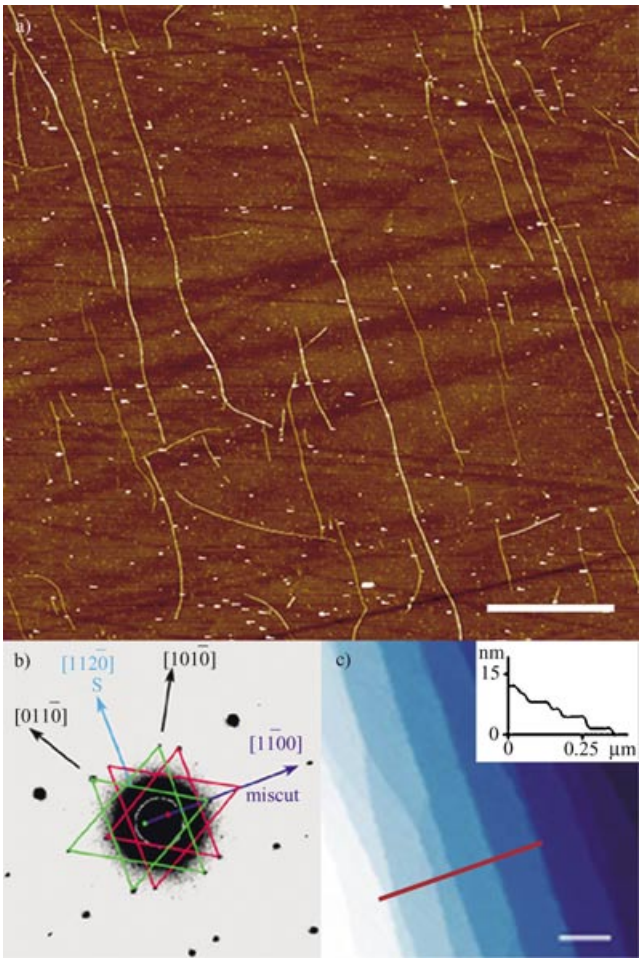

Figure 2. Comprehensive characterization of a typical sample of aligned SWNTs on miscut sapphire. a) AFM topographic image of the SWNTs (scale bar: 1 μm). Note the high degree of alignment and the straight conformation of most SWNTs, beyond the persistence length (ca. 1 μm). Polishing scratches (randomly oriented dark lines) of approximately 1-nm depth do not affect SWNT alignment. b) Asymmetric double-exposure back-reflection XRD indicating relevant low-index directions and the resulting step vector ($\mathbf{s}$). The green and red triangles indicate the reference reflections arising from the first exposure (2 h) and second exposure (1 h, after 180° sample rotation), respectively (see Supporting Information for reference XRD). The $\mathbf{s}$ vector is +90° from the vector connecting the green-to-red pattern centers. c) AFM topographic image of a piece of sample after annealing at 1100 °C (scale bar: 100 nm). The darker blue indicates lower terraces, whose edges correspond to the c–$3c$ macrosteps. The inset shows a section analysis along the red line. Note that both the $\mathbf{s}$ vector from (b) and the macrosteps from (c) are parallel to the SWNTs in (a) (all the images are displayed in the same orientation with respect to reference marks).

Interestingly, certain samples show kinked nanotubes running in zigzags along two different low-index directions. In Figure 4a, alternating long and short segments of the same

 © 2004 Wiley-VCH Verlag GmbH & Co. KGaA, Weinheim

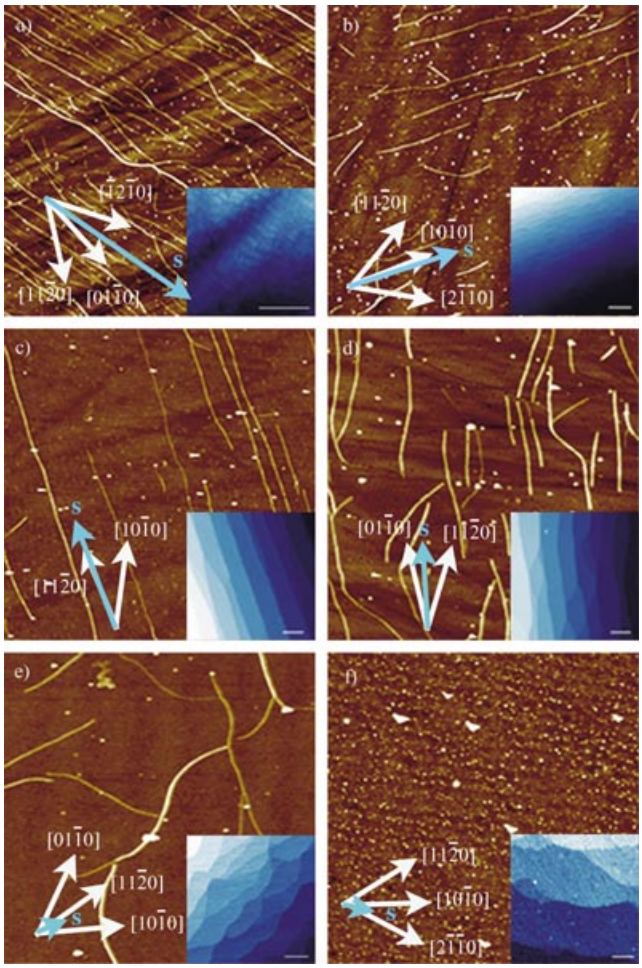

Figure 3. SWNTs on miscut sapphire. Comparative analysis of representative samples with different miscut inclination and azimuth angles (see Supporting Information for XRD and full data table): a) $\theta = 3.4 \pm 0.3°$, $\phi = 42 \pm 5°$; b) $\theta = 2.3 \pm 0.2°$, $\phi = -33 \pm 5°$; c) $\theta = 2.1 \pm 0.2°$, $\phi = 0 \pm 5°$; d) $\theta = 1.7 \pm 0.1°$, $\phi = 18 \pm 5°$; e) $\theta = 0.4 \pm 0.2°$, $\phi = -5 \pm 5°$; and f) $\theta = 0.3 \pm 0.2°$, $\phi = -50 \pm 5°$ (image sizes are 2.5 μm, except (e), 5 μm). The vectors indicate the relevant lattice directions and the step vector **s** (blue) obtained from XRD (except in (e) and (f), where **s** is from AFM). Insets show AFM topographic images of the respective annealed samples (inset scale bars 100 nm) with macrosteps. In (f), the atomic steps are spaced enough to be observed, and are decorated with inactive catalyst nanoparticles.

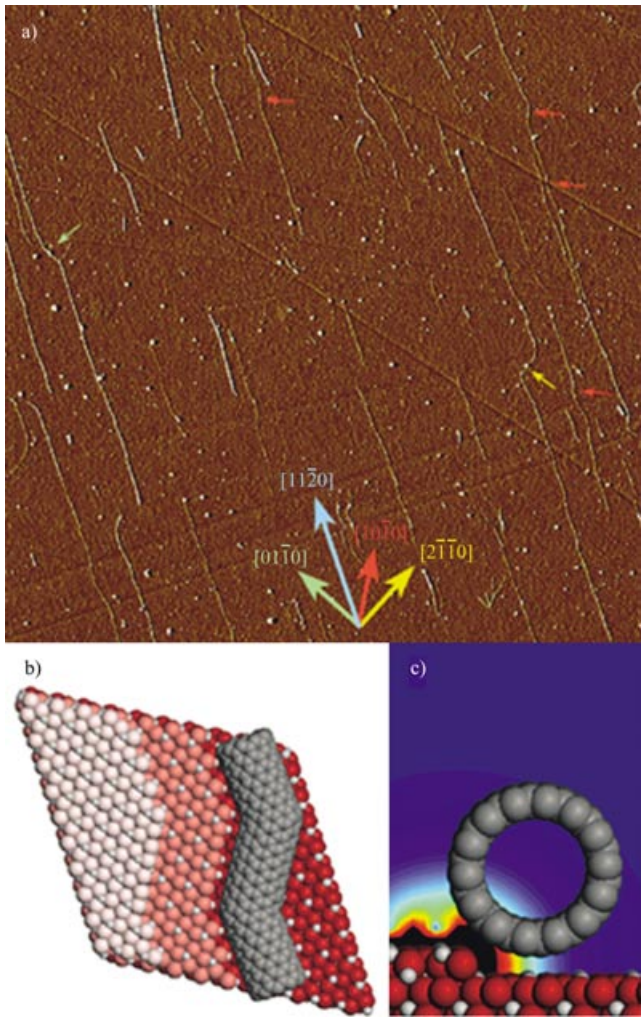

Figure 4. SWNT growth along atomic steps. a) AFM amplitude image of kinked SWNTs growing along the [11$\bar{2}$0] direction (blue) with short segments along the [10$\bar{1}$0] direction (red), and occasionally [2$\bar{1}\bar{1}$0] (yellow) and [01$\bar{1}$0] (green; image size 5 μm). The short arrows in the respective color point to a few such segments. b) Illustration of a (10,0)-(6,6)-(10,0) kinked nanotube along [11$\bar{2}$0]-[10$\bar{1}$0]-[11$\bar{2}$0]. c) Model of a 1-nm-diameter SWNT along a [11$\bar{2}$0] atomic step. The color gradient represents an estimated SWNT–step electrostatic interaction energy per unit of nanotube length as a function of SWNT axis position, $U(x,z)$. This was calculated from the force exerted on a polarizable body by an inhomogeneous field, $\mathbf{F} = (\alpha \mathbf{E} \cdot \nabla)\mathbf{E}$. Averaging the potential along the direction of the step and the SWNT (y) gives $U(x,z) = -\frac{1}{2}\alpha_{xx}E^2(x,z)$, where α_{xx} is the transverse polarizability of the SWNT per length[31] and $E(x,z)$ is the local field. The latter was derived from the unreconstructed atomic step, by summation of Coulomb potentials from bulk Mulliken charges, averaged along the y axis and corrected for slab edge effects by subtracting a similar potential without the step. (The blue-to-red scale is 0–750 eV nm^{-1}.)

SWNTs run along the [11$\bar{2}$0] and [10$\bar{1}$0] directions, respectively, in accordance with their proximity to the general step direction (a few segments along the [01$\bar{1}$0] and [2$\bar{1}\bar{1}$0] directions are occasionally seen too). This result can be attributed to SWNT growth along faceted atomic steps (Figure 4b). Since the sharp 30° kinks presumably occur during growth, they could involve pentagon–heptagon defects, which are an energetically favored alternative to bending or buckling. The energy associated with pentagon–heptagon defects was calculated to be about 7 eV,[26] whereas the minimum strain energy required to produce a 30° buckle in a 1-nm-dimater SWNT was estimated to be about 13 eV.[27] Single-nanotube Raman spectra from these samples exhibit a high intensity of D-band peaks, which indicates a significant loss of translational symmetry, that is consistent with this picture. Pentagon–heptagon defects are known to cause structural changes along the SWNTs,[28] thus producing interesting metal–semiconductor heterojunctions.[29] In addition, the right-handedness of the kinked nanotubes reveals the chirality of the miscut substrate, which could in principle distinguish between enantiomorphic SWNTs. A different intriguing aspect is that faceting of vicinal α-Al_2O_3(0001)

 © 2004 Wiley-VCH Verlag GmbH & Co. KGaA, Weinheim

atomic steps has not yet been observed,[22] because of their relatively low anisotropy energy below $\theta = 1°$. The anisotropy is expected to increase at higher miscut inclinations as a result of step–step interactions, but could not be resolved by AFM. Here, the decoration by SWNTs reveals a faceting that would otherwise remain unseen.

We propose a "wake-growth" mechanism to describe the atomic-step-templated formation of SWNTs, in which the catalyst nanoparticle slides along the atomic step and leaves the growing SWNT behind as a wake. This would involve three main factors: 1) higher nanotube-surface van der Waals (vdW) interactions near the step that result from increased contact area; 2) electrostatic interaction between the local electric fields created by uncompensated dipoles at the atomic steps and the induced dipoles across the SWNTs; and 3) better wetting of the atomic steps by the Fe metal catalyst nanoparticles, because of capillarity and higher coordination. The vdW contribution to the interaction energy per unit of nanotube length can be theoretically extrapolated from previous calculations on Si surfaces ($2.2\ \mathrm{eV\,nm^{-1}}$),[30] by assuming proportionality with the substrate polarizability[31] and a Clausius–Mossotti relation,[31] which yields $1.4\ \mathrm{eV\,nm^{-1}}$ on SiO_2 and $2.2\ \mathrm{eV\,nm^{-1}}$ on α-Al_2O_3 surfaces. This small difference cannot account for the results in Figures 1 a and b. Moreover, the lack of alignment by the approximately 1-nm-deep polishing scratches (Figure 2 a) suggests that vdW interactions may not be the only aligning factor. On the other hand, electrostatic interactions may be especially high as a result of the ionic character of α-Al_2O_3. The electrostatic nanotube–step interaction was modeled, as a first approximation, by applying theoretical SWNT polarizabilities[32] and a Coulomb potential near an unreconstructed step (Figure 4 c). This electrostatic interaction is about $50\ \mathrm{eV\,nm^{-1}}$ at a reasonable vdW distance (0.34 nm) from the step. Although this remarkable value should be diminished by surface relaxation and reconstruction, it may still significantly account, along with vdW forces, for the strong SWNT–Al_2O_3 interaction compared to that of SWNT–SiO_2 (Figure 1 a,b), as well as for the high degree of nanotube alignment along the atomic steps.

The present study shows that atomic-scale surface features can direct the orientation and conformation, and possibly also the structure, of single-wall carbon nanotubes. The direction and morphology of the atomic steps can be macroscopically controlled in the crystal cutting process by two degrees of freedom, namely the miscut inclination θ and azimuth ϕ. Although the nanotubes are not yet regularly spaced, the atomic steps are. Therefore, an improved catalyst should in principle be able to yield periodic arrays of SWNTs with controllable spacing. Lastly, step-templated assembly may not be limited to carbon nanotubes and vicinal surfaces, but could be generally applicable to other axial-growth nanowires as well as to other controllable surface defects, such as etch pits, grain boundaries, and screw dislocations. This will enable new strategies for the large-scale fabrication of nanoscale devices from the bottom up.

Keywords: crystal engineering · nanostructures · nanotechnology · nanotubes · surface chemistry

[1] M. S. Strano, C. A. Dyke, M. L. Usrey, P. W. Barone, M. J. Allen, H. W. Shan, C. Kittrell, R. H. Hauge, J. M. Tour, R. E. Smalley, *Science* **2003**, *301*, 1519 – 1522.

[2] R. Krupke, F. Hennrich, H. von Lohneysen, M. M. Kappes, *Science* **2003**, *301*, 344 – 347.

[3] E. Joselevich, *Angew. Chem.* **2004**, *116*, 3052 – 3054; *Angew. Chem. Int. Ed.* **2004**, *43*, 2992 – 2994.

[4] X. F. Duan, Y. Huang, Y. Cui, J. F. Wang, C. M. Lieber, *Nature* **2001**, *409*, 66 – 69.

[5] P. Avouris, *Acc. Chem. Res.* **2002**, *35*, 1026 – 1034.

[6] *Nanoelectronics and Information Technology* (Ed.: R. Waser), Wiley-VCH, Weinheim, **2003**.

[7] Y. N. Xia, P. D. Yang, Y. G. Sun, Y. Y. Wu, B. Mayers, B. Gates, Y. D. Yin, F. Kim, Y. Q. Yan, *Adv. Mater.* **2003**, *15*, 353 – 389.

[8] E. Joselevich, C. M. Lieber, *Nano Lett.* **2002**, *2*, 1137 – 1141.

[9] A. Ural, Y. M. Li, H. J. Dai, *Appl. Phys. Lett.* **2002**, *81*, 3464 – 3466.

[10] S. M. Huang, B. Maynor, X. Y. Cai, J. Liu, *Adv. Mater.* **2003**, *15*, 1651 – 1655.

[11] Y. Huang, X. F. Duan, Q. Q. Wei, C. M. Lieber, *Science* **2001**, *291*, 630 – 633.

[12] M. R. Diehl, S. N. Yaliraki, R. A. Beckman, M. Barahona, J. R. Heath, *Angew. Chem.* **2002**, *114*, 363 – 366; *Angew. Chem. Int. Ed.* **2001**, *41*, 353 – 356.

[13] N. A. Melosh, A. Boukai, F. Diana, B. Gerardot, A. Badolato, P. M. Petroff, J. R. Heath, *Science* **2003**, *300*, 112 – 115.

[14] W. A. Lopes, H. M. Jaeger, *Nature* **2001**, *414*, 735 – 738.

[15] M. P. Zach, K. H. Ng, R. M. Penner, *Science* **2000**, *290*, 2120 – 2123.

[16] H. Yan, S. H. Park, G. Finkelstein, J. H. Reif, T. H. LaBean, *Science* **2003**, *301*, 1882 – 1884.

[17] P. Gambardella, M. Blanc, H. Brune, K. Kuhnke, K. Kern, *Phys. Rev. B* **2000**, *61*, 2254 – 2262.

[18] S. Iijima, *Nature* **1991**, *354*, 56 – 58.

[19] D. G. Dresselhaus, A. P. Dresselhaus, *Carbon Nanotubes: Synthesis, Properties, and Applications*, Springer, Heidelberg, **2004**.

[20] S. Helveg, C. Lopez-Cartes, J. Sehested, P. L. Hansen, B. S. Clausen, J. R. Rostrup-Nielsen, F. Abild-Pedersen, J. K. Norskov, *Nature* **2004**, *427*, 426 – 429.

[21] M. Su, Y. Li, B. Maynor, A. Buldum, J. P. Lu, J. Liu, *J. Phys. Chem. B* **2000**, *104*, 6505 – 6508.

[22] O. Kurnosikov, L. P. Van, J. Cousty, *Surf. Sci.* **2000**, *459*, 256 – 264.

[23] G. A. Somorjai, *Chem. Rev.* **1996**, *96*, 1223 – 1235.

[24] J. R. Heffelfinger, M. W. Bench, C. B. Carter, *Surf. Sci.* **1997**, *370*, L168 – L172.

[25] C. Barth, M. Reichling, *Nature* **2001**, *414*, 54 – 57.

[26] J. Han, M. P. Anantram, R. L. Jaffe, J. Kong, H. Dai, *Phys. Rev. B* **1998**, *57*, 14983 – 14989.

[27] B. I. Yakobson, C. J. Brabec, J. Bernholc, *Phys. Rev. Lett.* **1996**, *76*, 2511 – 2514.

[28] M. Ouyang, J. L. Huang, C. L. Cheung, C. M. Lieber, *Science* **2001**, *291*, 97 – 100.

[29] Z. Yao, H. W. C. Postma, L. Balents, C. Dekker, *Nature* **1999**, *402*, 273 – 276.

[30] T. Hertel, R. E. Walkup, P. Avouris, *Phys. Rev. B* **1998**, *58*, 13870 – 13873.

[31] J. Israelachvili, *Intermolecular and Surface Forces*, Harcourt Brace & Company, San Diego, **1997**.

[32] L. X. Benedict, S. G. Louie, M. L. Cohen, *Phys. Rev. B* **1995**, *52*, 8541 – 8549.

Received: April 18, 2004

 © 2004 Wiley-VCH Verlag GmbH & Co. KGaA, Weinheim